Solid-State Electronics 200 (2023) 108536

Contents lists available at ScienceDirect

Solid State Electronics

journal homepage: www.elsevier.com/locate/sse

Discontinuous Galerkin concept for Quantum-Liouville type equations ☆

Valmir Ganiu *, Dirk Schulz

Chair for High Frequency Techniques, TU Dortmund, Dortmund, Germany

ARTICLE INFO

Keywords:
Computational nanotechnology
Numerical methods
Quantum transport
Von-Neumann equation
Quantum Liouville type equation

ABSTRACT

A time-dependent discontinuous Galerkin method for the numerical solution of the Liouville–von-Neumann equation in center mass coordinates for the analysis of quantum transport in nanoelectronics and nanophotonics systems is presented. With this methodology, a further increase in computational efficiency compared to conventional methods is achieved, particularly when considering large-scale problems.

1. Introduction

The full potential of Wigner function approaches is emerging for the analysis of quantum electronic devices [1]. Recently, a closely related method for the analysis of the carrier transport within quantum devices was proposed that starts from the Liouville–von Neumann equation in center-mass coordinates and applies a Finite Volume (FV) method for the spatial approximation [2]. After an expansion of the density matrix according to predefined eigenfunctions, an equation is obtained, which corresponds to the conventional Wigner Transport Equation (WTE) [1]. With this method, also called Quantum Liouville type equation (QLTE), suitable boundary conditions to account for open systems are incorporated by the introduction of a complex potential [2].

Instead of choosing the FV technique, an approximation applying Finite Element (FE) techniques would be conceivable. For time-dependent problems, the use of FV schemes or even conceivable FE techniques require the solution of large equation systems. Thus, such algorithms can be exceedingly computationally expensive.

Alternatively, discontinuous Galerkin (DG) methods have proven themselves in fluid dynamics to be computationally efficient [3,4] as they bypass the solution of linear equation systems and allow high performance computation via parallelizable matrix–vector multiplications. Due to the mathematical relationship of the initial master equations, e.g. Navier–Stokes equations [5] and QLTE, the DG methodology seems to be a suitable technique for the approximation of QLTEs.

The DG approach is applied onto the mentioned QLTE [2], validated and its computational efficiency is evaluated for its application onto the simulation of quantum transport problems.

2. Discontinuous Galerkin approach

The framework is the Liouville–von-Neumann equation (LVNE) utilizing a spatially constant effective mass Hamiltonian and a Hartree–Fock potential. The LVNE is first transformed into center-mass coordinates χ and ξ yielding the following expression [6]:

$$\frac{\partial}{\partial t}\rho(\chi,\xi,t) = \imath\frac{\hbar}{m}\frac{\partial}{\partial\chi}\frac{\partial}{\partial\xi}\rho(\chi,\xi,t) - \imath\frac{q}{\hbar}G(\chi,\xi,t)\rho(\chi,\xi,t). \tag{1}$$

Here, ρ denotes the statistical density matrix and the term G includes the potential energy V, which contains the Hartree–Fock potential and the externally applied bias [7]. In detail, the term G is defined as [6]

$$G(\chi,\xi,t) = V\left(\chi+\frac{1}{2}\xi,t\right) - V\left(\chi-\frac{1}{2}\xi,t\right) - \imath W(\xi). \tag{2}$$

To suppress artificial reflections at boundaries in ξ-direction, a complex absorbing potential $\imath W(\xi)$ as described in [6] is introduced in (2). Eq. (1) is then approximated with respect to the coordinate ξ utilizing a finite volume technique with an equidistant grid characterized by an even number of N_ξ cell points symmetrically distributed around $\xi = 0$. Alternatively, the DG method could be applied. However, in doing so, one has to take into account that a thorough investigation of the numerical flux in χ-direction cannot be done, since a second numerical flux for the ξ domain is needed. The resulting relation is conceptually characterized by matrices $\widetilde{\boldsymbol{A}}$ and $\widetilde{\boldsymbol{G}}$ [6], both showing a dimension of $N_\xi \; x \; N_\xi$:

$$\frac{\partial}{\partial t}\boldsymbol{\rho}(\chi,t) = \widetilde{\boldsymbol{A}}\frac{\partial}{\partial\chi}\boldsymbol{\rho}(\chi,t) - \widetilde{\boldsymbol{G}}(\chi,t)\boldsymbol{\rho}(\chi,t) \tag{3}$$

Ultimately, a basis transformation is required to allow a distinction between forward and backward propagating waves. Thus, basis vectors $\boldsymbol{\Phi_n}$ together with their expansion functions $c(\chi,t)$ are introduced.

☆ The review of this paper was arranged by Francisco Gamiz.

* Corresponding author.
E-mail addresses: valmir.ganiu@tu-dortmund.de (V. Ganiu), dirk2.schulz@tu-dortmund.de (D. Schulz).

https://doi.org/10.1016/j.sse.2022.108536

Available online 21 November 2022

The basis vectors are orthonormal, such that $\boldsymbol{\Phi}_n^\dagger \cdot \boldsymbol{\Phi}_m = \delta_{n,m}$ holds. Accordingly, the transformation

$$\boldsymbol{c}(\chi,t) = \boldsymbol{\Phi}^\dagger \cdot \boldsymbol{\rho}(\chi,t) \tag{4}$$

is applied by introducing the matrix $\boldsymbol{\Phi}$ containing the basis vectors $\boldsymbol{\Phi}_n$. Exploiting the transformation (4), the QLTE reads as

$$\frac{\partial}{\partial t}\boldsymbol{c}(\chi,t) = \boldsymbol{\Phi}^\dagger \widetilde{\boldsymbol{A}} \boldsymbol{\Phi} \frac{\partial}{\partial \chi}\boldsymbol{c}(\chi,t) - \boldsymbol{\Phi}^\dagger \widetilde{\boldsymbol{G}}(\chi,t)\boldsymbol{\Phi} \cdot \boldsymbol{c}(\chi,t) \tag{5}$$

with $\boldsymbol{\Lambda} = \boldsymbol{\Phi}^\dagger \widetilde{\boldsymbol{A}} \boldsymbol{\Phi}$ being a diagonal matrix containing the eigenvalues λ_j of the matrix $\widetilde{\boldsymbol{A}}$ when the basis vectors $\boldsymbol{\Phi}_n$ are its eigenvectors.

To solve (5), the DG concept is applied, whereas the computational domain Ω_χ ($[0, L_\chi]$) is subdivided in elements denoted by k. Each component $c_j(\chi,t)$ of the vector $c(\chi,t)$ is expanded based on a nodal element approach with N_p nodal points for each element k. Test functions $l_i(\chi)$ of the order $N = N_p - 1$ must be introduced and (5) is multiplied with each of the defined test functions $l_m(\chi)$. The resulting relations are integrated with respect to χ for each element k. Additionally, a similar nodal expansion of the matrix element functions $\widetilde{G}_{jp}(\chi) \cdot c_p(\chi)$ with regard to the matrix $\boldsymbol{\Phi}^\dagger \widetilde{\boldsymbol{G}}(\chi,t)\boldsymbol{\Phi}$ in (5) is applied. Contrary to conventional FE approaches, a single-valued numerical flux $f_j^{k,*}(\chi,t) = \lambda_j \cdot c_j^{k,*}(\chi,t)$ is introduced to establish the coupling between all elements. To arrive at the local strong formulation, (5) is integrated twice utilizing Green's theorem. The following expression is obtained for each element-related function $c_j(\chi,t)$:

$$\boldsymbol{M}^k \partial_t \boldsymbol{c}_j^k - \boldsymbol{S}^k \boldsymbol{f}_j^k + \boldsymbol{M}^k \sum_{p=1}^{N_\xi} \mathrm{diag}(\underline{\widetilde{\boldsymbol{G}}}_{jp}^k)\boldsymbol{c}_p^k$$

$$= \oint_{\partial D^k} (f_j^k(\chi,t) - f_j^{k,*}(\chi,t))\hat{n}\boldsymbol{l}(\chi). \tag{6}$$

As for standard FE approaches, a stiffness matrix $\boldsymbol{S}^k$ and a mass matrix $\boldsymbol{M}^k$ are introduced. The vectors $\boldsymbol{c}_p^k$ and $\boldsymbol{f}_p^k$ contain the nodal values for element k and the vector $\boldsymbol{l}(\chi)$ the test functions $l_i(\chi)$, respectively. The diagonal elements of $\mathrm{diag}(\underline{\widetilde{\boldsymbol{G}}}_{jp}^k)$ contain the nodal values of the matrix element functions G_{jp}^k. The term on the right-hand side of (6) is approximated assuming an upwind flux according to

$$\oint_{\partial D^k} (f_j^k(x,t) - f_j^{k,*}(x,t))\hat{n}\underline{l}(x)$$

$$= \left(\frac{\lambda_j - |\lambda_j|}{2}\right)\hat{n}_r^-[[u]]_r\boldsymbol{e}_r - \left(\frac{\lambda_j + |\lambda_j|}{2}\right)\hat{n}_l^-[[u]]_l\boldsymbol{e}_l. \tag{7}$$

with $\boldsymbol{e}_r = (0,\ldots,0,1)^T$ and $\boldsymbol{e}_l = (1,0,\ldots,0)^T$. Here $\hat{n}_{r/l}^-$ denote face normals pointing from the edges of an element to its interior and the values $[[u]]_{r/l} = \hat{n}^- c^- + \hat{n}^+ c^+$ indicate the jumps, whereas $c^{-/+}$ are the interior and exterior values and $n^{-/+}$ are the corresponding face normals with regard to the edges of the element, respectively. The inflow and outflow boundary conditions are set according to Fermi statistics. Finally, along with the use of (7), the relation (6) for each expansion function $c_j(\chi,t)$ applied onto each element can be assembled to arrive at the system equation.

3. Validation and computational efficiency

To validate the approach, a RTD device as shown in Fig. 1 is chosen. The computational domains in χ and ξ-direction are $L_\chi = 60$ nm and $L_\xi = 100$ nm, respectively. Furthermore, the χ-domain is divided into $N_\chi = 60$ elements, where each χ-element is further characterized by $N_p = 3$ nodal points, while $N_\xi = 120$ is the number of cells in ξ-direction. For thermal equilibrium and assuming a flatband case, the real part and the imaginary part of the statistical density matrix are calculated and shown in Fig. 2 and Fig. 3, respectively. The results depicted are in good agreement with the results shown in [7]. Particularly, the real part of the density matrix matches with the results obtained in [7]. Upwind fluxes cause minor deviations in the imaginary part of the statistical density matrix (Fig. 4) as explained in [7], which should be theoretically zero for thermal equilibrium. The error is a consequence of the overestimation of diffusion effects [7]. As such, the integral contributor to the occurring error is caused by the approximation of the diffusion term $\widetilde{\boldsymbol{A}}\frac{\partial}{\partial\chi}\boldsymbol{\rho}(\chi,t)$ in (3) and can be alleviated by increasing the number of elements in χ-direction. Fig. 4 shows that the imaginary part of the statistical density matrix is reduced by a magnitude of 10, when the number of discretization elements N_χ and N_ξ are doubled. As a consequence, the error converges to zero when applying a finer discretization in χ-direction. Further optimization can be undertaken according to [8]. Finally, the DG scheme is conceptually suited for solving the QLTE. To demonstrate the computational efficiency, computation times of the DG-approach are compared to those of an FV-approach, for which linear equation systems have to be solved. Particularly the transient solution is of interest, as with the time dependent case the switching behavior and non-linear effects can be analyzed. The transient solution of the DG approach was calculated utilizing the second order (RK2) and fourth order (RK4) method, respectively. To assess the stability of both methods, the eigenvalues of the time dependent system matrix containing an upwind

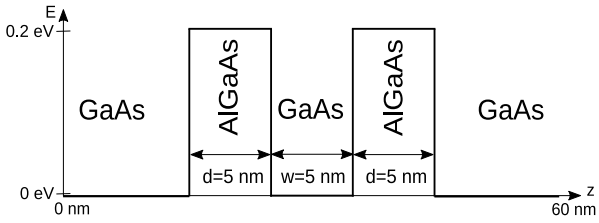

Fig. 1. Schematic of the RTD under investigation.

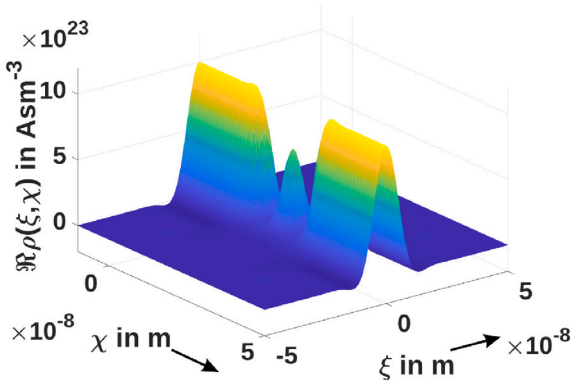

Fig. 2. Real part of the statistical density matrix ρ.

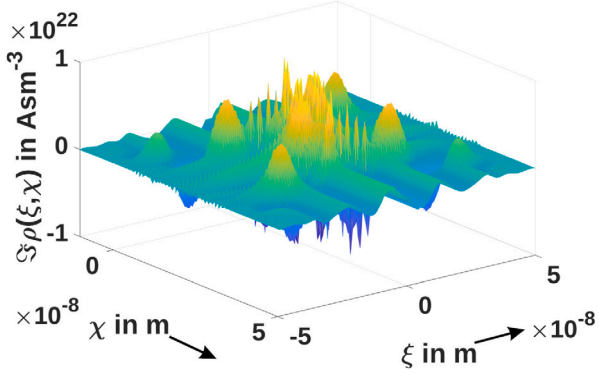

Fig. 3. Imaginary part of the statistical density matrix ρ.

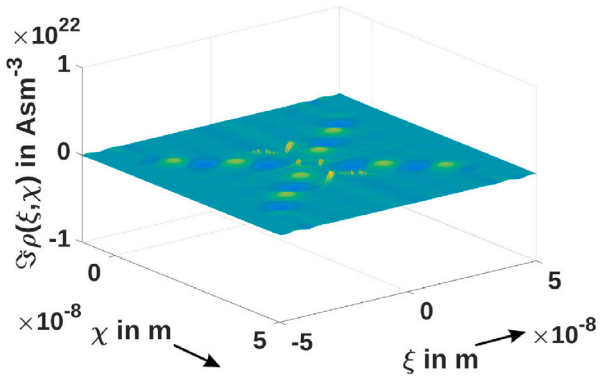

Fig. 4. Imaginary value of the statistical density matrix ρ for $N_\xi = 240$, $N_\chi = 120$.

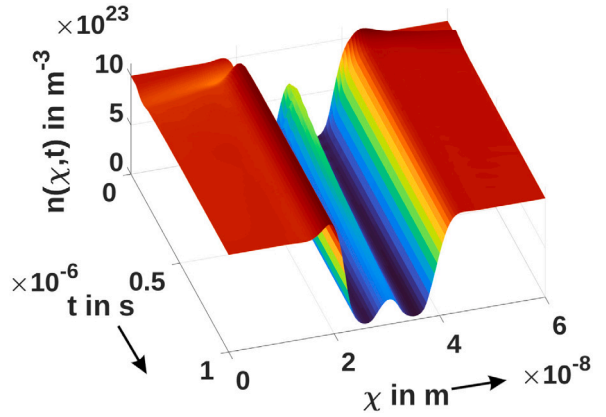

Fig. 5. Spatially time dependent carrier density n.

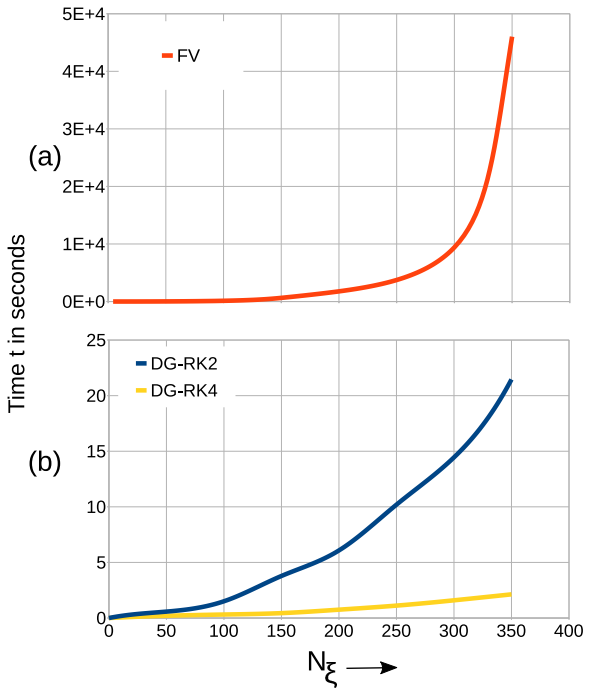

Fig. 6. Computational time for the FV method (a) as well as for the Runge Kutta methods RK2 and RK 4 (b).

flux were analyzed. The complex absorbing potential leads to a decay of the distribution function at the edges of the computational domain [2] and, therefore, enforces the appearance of an eigenvalue spectrum with eigenvalues consisting of purely negative real parts. To allow for an objective comparison, the average computation time for each time step for the transient solution is calculated. The number of discretization elements has a major impact on the computation time. Accordingly, as for example, the number of ξ-elements will be varied between 50 and 350, in 50 block increments for the FV-approach, RK2, and RK4 method. The previously mentioned parameters L_χ, L_ξ, N_χ, and N_p remain unchanged. The transient simulation starts with the density matrix in thermal equilibrium (see Fig. 2) and converges to the statistical density matrix under the assumption of an externally applied bias of 0.2 V under steady state conditions, when a time dependent step function is applied for the external bias having an amplitude of 0.2 V. This statement can be concluded from the evolution of the carrier density over time as shown in Fig. 5, which can be extracted from the diagonal of the statistical density matrix for each time step. Depending on N_ξ, the progression of the computation time for the FV methodology is exponential (Fig. 6a). Similarly, the RK2 method progresses exponentially with the increase of N_ξ, although the rate is not as pronounced as in the FV scheme and the RK4 algorithm shows a more linear trajectory (Fig. 6b). Due to the fact that the DG approach allows the application of an explicit method for the calculation of the transient solution, the RK2 and RK4 method show a decrease in computation time compared to the FV methodology, which requires the application of implicit methods.

4. Conclusion and outlook

The DG methodology achieves satisfactory results compared to other conventional methods for solving carrier transport problems, while significantly reducing the computation time especially for transient problems.

Declaration of competing interest

The authors declare that they have no known competing financial interests or personal relationships that could have appeared to influence the work reported in this paper.

Data availability

Data will be made available on request.

Acknowledgment

This work was supported by the Deutsche Forschungsgemeinschaft DFG under Grant SCHU 1016/10-1.

References

[1] Weinbub J, Ferry DK. Recent advances in wigner function approaches. Appl Phys Rev 2018;5(4):041104. http://dx.doi.org/10.1063/1.5046663.
[2] Schulz L, Schulz D. Numerical analysis of the transient behavior of the non-equilibrium quantum Liouville equation. IEEE Trans Nanotechnol 2018;(6):1197–205. http://dx.doi.org/10.1109/TNANO.2018.2868972.
[3] Cockburn B. Discontinuous Galerkin methods for computational fluid dynamics. In: Encyclopedia of computational mechanics. 2nd ed. John Wiley And Sons, Ltd; 2017, p. 1–63. http://dx.doi.org/10.1002/9781119176817.ecm2053.
[4] Peraire J, Persson P-O. High-order discontinuous Galerkin methods for CFD. Adapt High-Order Methods Comput Fluid Dyn 2011;2:119. http://dx.doi.org/10.1142/9789814313193_0005.
[5] Karakashian O, Katsaounis T. A discontinuous Galerkin method for the incompressible Navier-Stokes equations. 2000, p. 157–66. http://dx.doi.org/10.1007/978-3-642-59721-3_11.
[6] Schulz L, Inci B, Pech M, Schulz D. Subdomain-based exponential integrators for quantum Liouville-type equations. J Comput Electron 2021;20(6):2070–90. http://dx.doi.org/10.1007/s10825-021-01797-2.
[7] Schulz D, Mahmood A. Approximation of a phase space operator for the numerical solution of the wigner equation. IEEE J Quantum Electron 2016;52(2):1–9. http://dx.doi.org/10.1109/JQE.2015.2504086.
[8] Fu G, Shu C-W. Optimal energy-conserving discontinuous Galerkin methods for linear symmetric hyperbolic systems. J Comput Phys 2019;394:329–63. http://dx.doi.org/10.1016/j.jcp.2019.05.050, URL https://www.sciencedirect.com/science/article/pii/S0021999119304024.